Dynamics of Nanoscopic Water: Vibrational Echo and Infrared Pump−Probe Studies of Reverse Micelles†

Ivan R. Piletic, Howe-Siang Tan, and M. D. Fayer*

Department of Chemistry, Stanford University, Stanford, California 94305

Received: April 8, 2005; In Final Form: May 12, 2005

The dynamics of water in nanoscopic pools 1.7−4.0 nm in diameter in AOT reverse micelles were studied with ultrafast infrared spectrally resolved stimulated vibrational echo and pump−probe spectroscopies. The experiments were conducted on the OD hydroxyl stretch of low-concentration HOD in the H_2O, providing a direct examination of the hydrogen-bond network dynamics. Pump−probe experiments show that the vibrational lifetime of the OD stretch mode increases as the size of the reverse micelle decreases. These experiments are also sensitive to hydrogen-bond dissociation and reformation dynamics, which are observed to change with reverse micelle size. Spectrally resolved vibrational echo data were obtained at several frequencies. The vibrational echo data are compared to data taken on bulk water and on a 6 M NaCl solution, which is used to examine the role of ionic strength on the water dynamics in reverse micelles. Two types of vibrational echo measurements are presented: the vibrational echo decays and the vibrational echo peak shifts. As the water nanopool size decreases, the vibrational echo decays become slower. Even the largest nanopool (4 nm, ∼1000 water molecules) has dynamics that are substantially slower than bulk water. It is demonstrated that the slow dynamics in the reverse micelle water nanopools are a result of confinement rather than ionic strength. The data are fit using time-dependent diagrammatic perturbation theory to obtain the frequency−frequency correlation function (FFCF) for each reverse micelle. The results are compared to the FFCF of water and show that the largest differences are in the slowest time scale dynamics. In bulk water, the slowest time scale dynamics are caused by hydrogen-bond network equilibration, i.e., the making and breaking of hydrogen bonds. For the smallest nanopools, the longest time scale component of the water dynamics is ∼10 times longer than the dynamics in bulk water. The vibrational echo data for the smallest reverse micelle displays a dependence on the detection wavelength, which may indicate that multiple ensembles of water molecules are being observed.

I. Introduction

In this paper, we present studies of the dynamics of water confined on nanometer length scales in reverse micelles, using ultrafast infrared vibrational echo techniques. The experiments directly examine the structural evolution of the hydrogen-bond networks of water "nanopools" in the centers of reverse micelles that are a few nanometers in diameter. We refer to water confined on nanometer length scales as "nanoscopic water". Water is fundamentally important in a multitude of physical and biological processes. Many of these processes involve water in confined nanoscopic environments, rather than its bulk form. Nanoscopic water is important in chemistry,[1] biology,[2] and geology.[3] For instance, ion-exchange processes, which are important in analytical chemistry, are mediated by water in the confines of ion-exchange resins.[1] The dynamics of constrained water in the vicinity of bio-macromolecules are believed to be responsible for many biological functions, such as molecular recognition and enzymatic catalysis.[2,4] The water nanopools in reverse micelles are used as nanoreactors[5] and for hydration studies of enzymatic activity.[6] Confined water occurs in the micropores of minerals such as zeolites[7] and in cells.[8] These environments may contain from millions to only a few tens of water molecules.

Liquids that are confined to nanoscopic dimensions exhibit distinct structural and dynamical characteristics from their bulk liquid phases.[9−13] The key feature of liquid water is its formation of dynamic hydrogen-bond networks that are responsible for water's unique properties.[14] Bulk water dynamics occur over a range of time scales, from tens of femtoseconds to several picoseconds.[15−22] These dynamics are complex and encompass elastic and inelastic interactions with the surrounding water molecules. Vibrational lifetimes, excitation transfer, dephasing and orientational correlation times are all observed to decay by ∼2 ps for bulk water.[20,23−25] This paper focuses on the influence of confinement on the vibrational lifetimes and dephasing dynamics of water that is confined on a length scale of a few nanometers. The observations are related to the evolution of the hydrogen-bond network. Because hydrogen bonds are relatively weak, compared to covalent bonds, they are constantly breaking and forming in liquid water, which results in a constantly evolving hydrogen-bond network. When boundaries of nanoscopic dimensions are imposed on an ensemble of water molecules, the hydrogen-bond network is modified and new interactions between water and the boundary layer occur. In experimental investigations[26,27] and molecular dynamics (MD) simulations[28,29] of such systems, two types of water molecules are typically identified. We will refer to these as "associated" and "core." The water molecules forming the layer at the boundary of the confining environment will have specific interactions with the headgroups of the reverse micelles. These

† Part of the special issue "Irwin Oppenheim Festschrift".

* Author to whom correspondence should be addressed. Phone: 650-723-4446, 650-725-3527. Fax: 650-723-4817. E-mail address: fayer@stanford.edu.

10.1021/jp051837p CCC: $30.25 © 2005 American Chemical Society
Published on Web 06/15/2005

are said to be associated with the headgroups. Associated waters are believed to have restricted mobility, relative to water molecules removed from the headgroups in the core of the reverse micelles. Water molecules in the core of the nanoscopic water pools are believed to have more bulklike characteristics. However, there is no direct experimental evidence that such segregated water environments exist. The associated and core water molecules are coupled through a hydrogen-bond network, and the influence of the associated waters may extend well past the boundary headgroup solvation layer. Because the dynamics of water are largely dependent on the hydrogen-bond network, structural differences between bulk and nanoscopic water will result in different dynamics.

Systems that have been studied to investigate confinement effects include sol−gel pores,[11] zeolites,[30] cyclodextrins,[13] and reverse micelles.[31] Reverse micelles are widely regarded as very useful model systems of water in confinement. A reverse micelle consists of amphiphilic surfactant molecules arranged so that they form a closed structure with polar or charged headgroups pointing inward, toward the polar phase (water in most cases), while hydrocarbon chains are pointing outward, toward the nonpolar phase. Reverse micelles self-assemble when appropriate amounts of surfactant, polar, and nonpolar solvents are mixed together. Reverse micelles formed from the sodium bis(2-ethylhexyl) sulfosuccinate (AOT) surfactant have been used extensively in experiments because they are spherical, monodispersed, and have sizes that can be easily varied from ∼1 nm to tens of nanometers.[32,33]

Aspects of the dynamics of AOT reverse micelles have been explored by various techniques. The dielectric response of AOT reverse micelles in CCl_4 and *n*-heptane have examined in the 0.01−20 GHz range.[34] The authors have attributed the observed 100 MHz relaxation (10 ns) to a combination of two diffusion mechanisms: reorientation of the reverse micelle and the "free" diffusion of completely hydrated AOT ion pairs. The dielectric properties in the terahertz spectral range (3−33 cm^{-1}) have also been reported.[35] A resonance was observed that is not present in bulk water samples and is dependent on the size of the reverse micelle. The authors attributed it to surface modes. Fourier transform infrared (FTIR) spectroscopy has been applied to study the hydroxyl[27,36,37] and librational modes[38] of confined water in reverse micelles. The spectra of the hydroxyl stretch show a pronounced blue shift as the size of the water nanopool becomes smaller.[27] However, because of inhomogeneous broadening, no dynamical information can be obtained from the line shapes.

The dynamics of water in reverse micelles on fast time scales have been examined by measuring time-dependent properties of a probe molecule. Time-resolved fluorescence Stokes shift measurements of dye molecules in reverse micelles show a substantial size dependence, with the Stokes shift slowing as the reverse micelle is made smaller.[31,39,40] Infrared (IR) pump−probe experiments on the azide ion confined in reverse micelles have measured the azide ion vibrational lifetime.[41] A significant increase of the lifetime of the azide ion is observed for the smallest reverse micelles. Polarization-resolved pump−probe studies of the same system showed that the orientational relaxation of azide was at least an order of magnitude slower than the reported lifetimes, which was interpreted as suggesting restricted mobility of water in reverse micelles.[42] Vibrational echo peak shift measurements have also been used to study the dephasing dynamics of the azide ion in AOT reverse micelles.[43] These dynamical experiments provide valuable insights; however, they can provide only indirect information on the dynamics of the water that comprise the interior of reverse micelles. It is difficult to relate measurements on probe molecules to details of the water dynamics.

There have been direct measurements of some aspects of the dynamics of water in reverse micelles. The decay of orientational anisotropy of pure water in AOT reverse micelles was examined using polarization-resolved transient grating experiments on the OH stretch.[44] However, the observed fast anisotropy decay was assigned to rapid excitation transfer of the excited hydroxyl stretch among water molecules in the reverse micelle. Recently, an IR experiment examined the transfer of vibrational excitation from water nanopools in reverse micelles into the surrounding solvent.[45] Inelastic neutron scattering experiments studied the dynamics of water in reverse micelles by obtaining the line shapes as a function of the scattering angle.[46] The results were compared to MD simulations, and information was obtained on orientational and translation motions.[46]

Very recently, two direct studies of water dynamics in AOT reverse micelles were performed using ultrafast infrared techniques. In one study, the orientational relaxation of water was probed as a function of reverse micelle size by measuring the anisotropy decay of the hydroxyl stretch, using frequency-resolved polarized pump−probe experiments.[47] The results were compared to simulations.[48] A brief report of a study that used ultrafast infrared spectrally resolved stimulated vibrational echo measurements on the hydroxyl stretch of water in AOT reverse micelles has been presented.[49]

Here, we present a detailed account of the vibrational echo experiments on AOT reverse micelles that have been reported previously,[49] including new frequency-dependent data, as well as vibrational pump−probe experiments that examine the population dynamics of the hydroxyl stretch. Vibrational echo spectroscopy[16−18,20,50−56] is uniquely capable of determining system dynamics by removing the inhomogeneous broadening contribution from the line shape[16,56−62] and tracking the underlying dynamics.[63,64] The properties of hydrogen-bond networks can be studied using IR spectroscopy of the hydroxyl stretching mode, because of the strong influence of the number and strength of hydrogen bonds on the hydroxyl stretch frequency.[21,57,65−68] A water molecule can form up to 4 hydrogen bonds of varying strengths; however, the number and strengths of the hydrogen bonds are not spectroscopically resolvable under the broad hydrogen-bonded hydroxyl stretch band.[21,57] The evolution of the hydrogen bond network consists of fluctuations in the number and strengths of hydrogen bonds. Vibrational echo spectroscopy of the hydroxyl stretch examines the time evolution of the hydroxyl stretch frequency, and, therefore, the time evolution of the structure of the hydrogen-bond network.

Ultrafast IR vibrational echo techniques have been applied extensively to the study of bulk water.[16−18,20,54−56,69] These experiments have been shown to be valuable for understanding bulk water dynamics. Within the assumption that the frequency fluctuations are reasonably well-characterized as Gaussian, the ensemble-averaged measurement of the vibrational frequency evolution is characterized by $C(t)$, which is the frequency−frequency correlation function (FFCF):[64]

$$C(t) = \langle \delta\omega(t)\delta\omega(0)\rangle \qquad (1)$$

where $\delta\omega(t)$ is the deviation of the frequency from the mean value. Using the FFCF, the vibrational echo observables can be calculated. Conversely, experiments can be used to determine the FFCF, and the experimentally determined FFCF can then be compared to the analogous FFCF for bulk water. In these experiments, the dilute OD hydroxyl stretch of HOD in H_2O is

investigated to eliminate vibrational excitation transport and to ensure that the absorption of the sample is not too high. Detailed simulations of water show that experiments on the OD stretch provide an accurate measurement of water dynamics.[70] Therefore, measurements on the OD stretch provide a method for examining the equilibrium structural dynamics of water without the influence of vibrational excitation transport, which occurs when the hydroxyl stretch of pure water is vibrationally excited. The FFCF for the OD stretch in bulk water has been determined using vibrational echo experiments and compared to FFCFs obtained from MD simulations.[18,20,69] Recent bulk water simulations produce results that are in almost-quantitative agreement with the experiments.[69,71] The simulations of bulk water make it possible to assign dynamics observed in the vibrational echo experiments on different time scales to specific structural motions. Using the Gaussian fluctuation approximation in the analysis of the reverse micelle experiments, it is possible to compare the results to those obtained in the bulk water experiments, because the same approximation was made.

AOT reverse micelles with water nanopool diameters of 4, 2.4, and 1.7 nm corresponding to ~1000, ~300, and ~50 water molecules, respectively, were studied. The pump−probe data are presented and analyzed to obtain the vibrational lifetimes. In addition, long-lived pump−probe signals are observed that have been identified in bulk water as resulting from a shift in equilibrium distribution of hydrogen bonds following energy deposition from vibrational relaxation.[23] In contrast to bulk water,[23] the long-lived signals in the reverse micelles decay on a time scale of tens of picoseconds. The magnitude of the long-lived signal and its decay constant are dependent on the size of the reverse micelle. Both time-dependent vibrational echo decays and vibrational echo peak shift measurements at several frequencies are presented and discussed. The data are compared to identical experiments conducted on bulk water and on a 6 M NaCl solution, which is used to examine the role of ionic strength in the water dynamics. The vibrational echo data are analyzed using diagrammatic time-dependent perturbation theory. The analysis gives the FFCFs for the different-sized water nanopools, which is compared to the FFCF obtained for bulk water.[69] The results show that even the largest nanopools studied have dynamics that are substantially different from bulk water and that the differences are not attributable to ionic strength. Analysis of the frequency dependence of the vibrational echo signals suggests that the dynamics in the smallest reverse micelles involve more than one subensemble of water molecules.

II. Experimental Procedures

Reverse micelle solutions were prepared with AOT, carbon tetrachloride (CCl_4), and water (all from Aldrich) without further purification. A 1 M stock solution of AOT in CCl_4 was prepared. Because of the hygroscopic nature of the surfactant, the residual water content in this stock solution was determined by a Karl−Fisher titration (~0.5 water molecules per headgroup).

The size of the water nanopool is determined by the ratio[72,73]

$$w_0 = \frac{[H_2O]}{[AOT]} \tag{2}$$

To prepare solutions of desired w_0 value, precise volumes of water (5% HOD in H_2O) were added to measured quantities of the stock solution. For the AOT/water/isooctane mixture, an empirical formula for the diameter of the nanoscopic water pool (d_{wp}) has been obtained using several different datasets.[73] A linear relationship given by $d_{wp} = 0.29w_0 + 1.1$ (nm) for w_0 values in the range of 2−20 nm applies for these mixtures. In the experiments described in this paper, CCl_4 was used instead of isooctane, and its affect on the size of the reverse micelles is assumed to be small, because experiments using different organic solvents show only small changes in the diameter of the reverse micelles.[74] For $w_o = 2$, 5, and 10 used in these experiments, the diameters of the water nanopools are 1.7, 2.6, and 4.0 nm respectively.

Copper sample holders housing two 3-mm CaF_2 windows separated by a Teflon spacer were used to retain the sample. The samples' peak OD stretch absorptions were 0.2−0.4 in a path length of 250 μm. All the experiments were conducted at room temperature.

The laser system used in these experiments consisted of a home-built Ti:sapphire oscillator and regenerative amplifier, followed by a Spectra Physics OPA and difference frequency stage. The 800-nm, ~90-fs pulses pump the OPA containing a single 3-mm BBO crystal that is double-passed, generating near-IR wavelengths. A 0.5-mm $AgGaS_2$ crystal is used to difference-frequency mix the near-IR wavelengths to produce the ~4 mm mid-IR pulses (~4 μJ/pulse). The pulses are characterized in the frequency domain by measuring their spectra with a monochromator. In all of the samples studied, the laser spectrum was tuned to match the peak of the OD stretch in the linear absorption spectrum. Because the laser spectrum overlaps with absorption from CO_2 in the air, the experimental apparatus after the generation of mid-IR pulses was purged with CO_2 scrubbed air. To determine the pulse duration in the sample, the three time-delayed mid-IR pulses that are used in the experiment are cross-correlated in a nonresonant sample that contains only CCl_4. All of the beams pass through the identical amount of optical material. The sign and magnitude of the chirp on the pulses is determined by frequency-resolving the nonresonant signal in a monochromator (FROG experiment). Calcium fluoride and germanium windows are placed in the beam prior to beam splitting, to compensate the group velocity dispersion, so that the chirp across ~250 cm^{-1} of the laser spectrum is 0 ± 4 fs. The result is 50-fs transform-limited pulses in the sample.

Several different types of nonlinear third-order experiments were conducted. In all experiments, there are three interactions of the sample with the radiation field, with wave vectors of $\vec{k}_1$,$\vec{k}_2$, and $\vec{k}_3$, regardless of whether there are two or three pulses involved. The resultant signals propagate in the $-\vec{k}_1 + \vec{k}_2 + \vec{k}_3$ direction. The signals are detected after they are routed through a monochromator by an InSb detector. The monochromator resolution is set at ~10 cm^{-1}. A small amount of the original mid-IR pulse is split off and used for shot-to-shot normalization. The outputs of signal and reference detectors are captured with gated integrators and digitized.

Pump−probe experiments were conducted to determine the population relaxation dynamics of the OD stretch. The pump pulse is ~10 times more intense than the probe pulse. The pump−probe experiments are also spectrally resolved. To measure the population dynamics without contributions from orientational relaxation,[47] the pump−probe signal is measured after the monochromator through a polarizer placed immediately in front of the detector. The time-dependent probe signals, with the probe pulse polarization parallel and perpendicular to the pump pulse, are independently measured. The population decay is obtained from the standard form,

$$P(t) = I_{\parallel} + 2I_{\perp} \tag{3}$$

Measurements of $I_{\parallel}$ and $I_{\perp}$ (normalized by the probe intensity) are used, rather than the magic angle, to avoid depolarization

that is caused by the monochromator grating, which does not diffract the two components equally as well as metallic mirrors that cause a linearly polarized beam to become elliptical if it is not purely *s* or *p* polarized.[75] Equation 3 gives the population dynamics independent of its functional form. As discussed below, and has been described in detail for bulk water,[23] vibrational relaxation can lead to changes in the distribution of hydrogen bonds that result in long-lived signals. Therefore, in addition to taking data on the 0−1 transition, pump−probe data are also collected on the 1−2 transition. The ground-state absorption, although not completely negligible, is quite small in this region. Therefore, the vibrational lifetime can be determined without interference from the long-lived signal.

In the stimulated vibrational echo experiments, the mid-IR laser pulse is split into three pulses of equal intensity, using AR-coated ZnSe beam splitters. These excitation pulses are time-delayed and focused into the sample cell in a phase-matched (boxcar) geometry. The interpulse delays between pulses 1 and 2, and between pulses 2 and 3, are designated as τ and T_w, respectively. Vibrational echo scans are collected as a function of τ, for a series of T_w values. We observed a temporal drift in the timing of our laser pulses that was attributed to temperature equilibration of the apparatus under purged CO_2 conditions. To correct for any drifts in the timing of pulses 1 and 2, which is particularly important for the vibrational echo peak shift measurements, the two-pulse frequency-integrated vibrational echo emanating in the $-\vec{k}_1 + 2\vec{k}_2$ direction was measured simultaneously with the spectrally resolved stimulated vibrational echo, using a separate MCT detector. The peak of this two-pulse vibrational echo provides an accurate measure of $\tau = 0$, permitting the elimination of timing drift (~10 fs) between the first two pulses. Any small drifts associated with the delay between pulses 2 and 3 are insignificant, because the smallest T_w step size was 100 fs.

Frequency resolution of the signal is advantageous, because it eliminates contributions from the 1−2 hydroxyl stretch transition,[76] which complicate the data analysis. In addition, data taken at different frequencies can be compared. The largest T_w delay is limited by the vibrational excited-state lifetime (T_1) of the chromophore, because the signal amplitude decays exponentially with the lifetime. For $T_w < 200$ fs, there is a nonresonant signal peaked at $\tau = 0$ fs, mainly from the CCl_4. The nonresonant signal prevents the shapes of the vibrational echo decays to be analyzed for $T_w < 200$ fs. However, because the nonresonant signal is narrow and the peak shifts at $T_w = 0$ are large, it is possible to obtain a reasonably accurate value of the $T_w = 0$ peak shifts.

III. Results and Discussion

A. Fourier Transform Infrared and Pump−Probe Experiments. The background subtracted FTIR spectra of the OD stretch mode in (from left to right) bulk water and the $w_0 = 10$, 5, and 2 reverse micelles are shown in Figure 1. The peak positions (cm^{-1}) and full width at half maximum (fwhm) values (cm^{-1}) for bulk water and the $w_0 = 10$, 5, and 2 reverse micelles are (2506, 170), (2539, 174), (2558, 160), and (2566, 156), respectively. Experiments will also be presented on a 6 M NaCl solution, which has a spectrum with a peak position of 2526 cm^{-1} and an fwhm of 149 cm^{-1}. The spectra shift to higher frequency (blue shift) and become narrower with decreasing w_0.[27,49] In bulk water, the broad hydroxyl stretch absorption band is composed of an inhomogeneous distribution of species, with more hydrogen bonds and stronger hydrogen bonds producing red shifts and fewer and weaker hydrogen bonds producing blue shifts.[14,21,22] If the trends in bulk water are followed in reverse micelles, the blue shift with decreasing nanopool size suggests a decrease in the equilibrium number of hydrogen bonds and/or a decrease in the average hydrogen bond strength. The red shift of the OH librational band with decreasing reverse micelle size has also been attributed to a weaker hydrogen-bond network.[38] However, unlike bulk water, reverse micelles have interfacial waters at the headgroup layer. As the size of the reverse micelle is reduced, the relative number of these interfacial waters increases. It is likely that interfacial waters have different hydroxyl stretch spectra from the core waters, because the hydroxyl stretch frequency is very sensitive to the nature and extent of hydrogen bonding. Different spectra associated with subensembles of water molecules, rather than changes in the number or strength of the hydrogen bonds, may be responsible for the blue shift as the size of the nanopool is reduced.

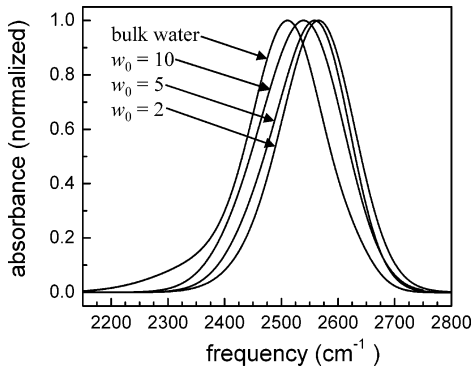

Figure 1. Fourier transform infrared (FTIR) spectra of the OD stretch of 5% HOD in H_2O in bulk water and $w_0 = 10$, 5, and 2 AOT reverse micelles.

A variety of FTIR experiments have tried to verify the existence of distinct water species in reverse micelles. The OH stretching modes of pure H_2O in reverse micelles have been studied.[27] Curve-fitting procedures have been applied on the pure OH band with the assumption that there are contributions arising from interfacial and bulklike water. These procedures suffer from a lack of uniqueness in fitting the spectra and the fact that the H_2O spectrum has contributions from the symmetric and antisymmetric stretches as well as the bending overtone.[36,37] The existence of an isosbestic point in the reverse micelle size-dependent FTIR spectra of the librational band of water (~600 cm^{-1}) suggests the possibility of two types of water, although the line shapes contain a good deal of inherent structure, particularly for the smallest reverse micelles.[38] From the absorption spectra displayed in Figure 1, it is impossible to decompose the spectra into several contributions arising from different "types" of water. The OD stretch of an HOD molecule is a local mode, and there is no Fermi resonance. The OD stretch line shape is a skewed Gaussian with a red tail that has no distinct structure or shoulders. In water, it has been shown that the transition dipole of the hydroxyl stretch increases as the frequency becomes lower, producing an asymmetric line shape.[77] The absorption spectra of the OD stretch of HOD in water nanopools in reverse micelles are consistent with water properties that vary continuously within a micelle for a given w_0.[36] However, the spectrum could also be composed of distinct species that have such broad and overlapping spectra that they are not resolved. The vibrational echo experiments presented below suggest that, at least for very small reverse micelles, water molecules exist with dynamical properties that vary with wavelength.

TABLE 1: Vibrational Lifetimes and Long-Lived Decay Times

sample	vibrational lifetime, T_1 (ps)	long-lived decay time, τ_r (ps)
bulk water	1.5	∞^a
$w_0 = 10$	2.6	180
$w_0 = 5$	4.4	100
$w_0 = 2$	6.3	20
6 M NaCl	3.4	∞^a

[a] No decay on the experimental time scale was exhibited.

IR pump−probe spectroscopy was used to measure vibrational lifetimes of the OD stretch mode of HOD in reverse micelles. As discussed in Section II, eq 3 was used to determine the lifetime. Table 1 contains the vibrational lifetimes (T_1) for the three reverse micelles, bulk water, and the NaCl solution. In hydrogen-bonded liquids, the vibrational lifetime is not trivial to measure, because the pump−probe experiment can be sensitive to spectral dynamics in the ground and excited state[62] and hydrogen bond dissociation,[69,78,79] in addition to vibrational relaxation. If a frequency-selected subset of the water molecules is excited by a relatively narrow pump pulse, then spectral diffusion in the ground and excited state will produce a frequency-dependent signal. This phenomenon has been used to explain pump−probe spectra[62] and the ultrafast IR−Raman spectroscopy of water.[80]

Recently, pump−probe experiments have been conducted on the OD stretch of HOD in bulk H_2O to examine the population dynamics.[23] To avoid the issues arising from spectral diffusion, the bandwidth of the IR pulses was large, compared to the absorption line width. The data displayed two contributions to the time dependence: the decay of the excited vibrations, followed by a shift in the equilibrium distribution of hydrogen bonds, because of the deposition of energy into the liquid.[23] The shift to a new distribution of hydrogen bonds produces "photoproducts" with a wavelength-dependent spectrum that is different from the initial spectrum. Comparison to FTIR, temperature difference spectra demonstrated that, within ~5 ps, the system reaches a new equilibrium distribution of hydrogen bonds, corresponding to a slightly elevated temperature. The production of photoproducts produces a wavelength-dependent long-lived change in the absorption spectrum. At the absorption maximum, the shift to a new distribution of hydrogen bonds results in a long-lived bleach that is constant on a 100-ps time scale.[23] Separation of the lifetime decay and the growth of the photoproducts gave a wavelength-independent OD stretch vibrational lifetime of 1.5 ps.[23] The data have the appearance of a fast decay to a nonzero constant pump−probe signal that is ~18% of the initial value of the signal. The constant component should decay on a very long time scale as heat diffuses out of the laser excitation volume. Because the bulk water samples were very thin (6 μm), the dominant heat flow pathway was into the CaF_2 windows, which takes ~10 μs. However, on the time scale of the experiments, the long-lived signal is constant.

Figure 2 displays pump−probe data spectrally resolved at the absorption maxima (0−1 transition) for each reverse micelle and bulk water. In addition to the data shown in Figure 2, data were taken at a wavelength 160 cm^{-1} to the red of the absorption maximum of each sample. The wavelength of 160 cm^{-1} is the anharmonicity of the OD stretch of HOD in water,[69] which is assumed to be the same for OD in the reverse micelles. Similar to that for bulk water, pump−probe decays measured at the peak of the 0−1 transition display a long-lived component that lasts for tens of picoseconds. However, in contrast to bulk water, the long-lived signal is not constant in time. In the reverse micelles, the long-lived signal decays with a decay constant that is dependent on the size of the reverse micelle.

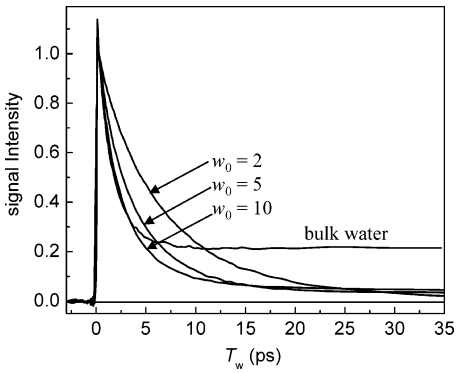

Figure 2. Pump−probe scans for bulk water, and $w_0 = 10$, 5, and 2 AOT reverse micelles frequency resolved at the absorption maximum for each sample.

The pump−probe experiments on the 1−2 transition measure the lifetime by examining the decay of the excited-state population out of the $v = 1$ level. Vibrational relaxation that results in the production of photoproducts in the ground state, in principle, will not influence the measurement of the lifetime when the 1−2 transition is probed. This is almost the case for the reverse micelles. The measurements made 160 cm^{-1} to the red of the 0−1 maximum decay almost to zero. There is still a very small long-lived component that is due to the overlap with the red tail of the 0−1 transition. The data were fit to an exponential decay plus a constant. Because the amplitude of the long-lived transition is very small, we can extract the vibrational lifetimes with little ambiguity. These lifetimes and the lifetimes of the bulk water are listed in Table 1. The vibrational lifetime determined for water is in agreement with recent work.[23] The lifetime measured in the same manner for the 6 M NaCl solution is also listed in Table 1. The NaCl solution will be discussed in connection with the vibrational echo data presented below.

Table 1 shows that the vibrational lifetimes become longer as the size of the reverse micelle decreases. It is not possible to explain the reason for this trend quantitatively, but there are qualitative considerations that may offer an explanation. Vibrational relaxation of a high-frequency mode will occur via anharmonic couplings to lower-frequency modes.[81] Generally, the lowest-order pathway (the one involving the fewest modes) will dominate the relaxation. Relaxation will occur via the population of internal modes when possible and then, to conserve energy, some number of quanta of the continuum of low-frequency intermolecular modes will be excited (or annihilated).[82] For the hydroxyl stretch of water, vibrational relaxation involves excitation of the bending mode.[80] In the reverse micelles, as the size decreases, the OD stretch shifts to higher frequency (see Figure 1). Studies of hydrogen-bonding systems show perturbations that shift the stretch to higher frequency and shift the bend to lower frequency.[83] If this is also the case in reverse micelles, as the reverse micelle becomes smaller, the energy difference between the stretch and the bend becomes larger, and more energy must be deposited into some combination of modes of the continuum. The nature of the modes of the continuum will change as the size decreases. If the coupling to the modes decreases and/or the density of states decreases, then the lifetime will increase. The continuum is even more complex for the reverse micelles, because surface modes are observed to occur at terahertz frequencies.[84]

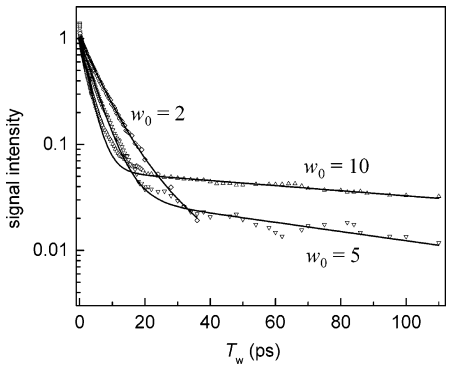

Figure 3. Long-time pump−probe scans for $w_0 = 10$, 5, and 2 AOT reverse micelles. Biexponential fits were used to obtain the hydrogen bond reformation time scales (τ_r) listed in Table 1 (see text).

However, there is no simple rule to predict the lifetime of the OD stretch based solely on its frequency. The 6 M NaCl solution absorbs at 2525 cm^{-1}, which occurs at a lower frequency than the $w_0 = 10$ sample (2535 cm^{-1}), but the OD stretch in the NaCl solution has a longer lifetime (3.4 ps vs 2.5 ps) than it does in the reverse micelle. As is discussed below in association with the vibrational echo experiments, in the reverse micelles, the Na^+ counterions are mainly associated with negatively charged headgroups, and the nanopool water has a low ionic strength, compared to 6 M NaCl. The nature of water in salt solutions is substantially different than bulk water,[85] and, as shown below, it is also different from nanoscopic water in reverse micelles. The relaxation pathways, coupling constants, and density of states of low-frequency modes in the salt solution could be quite different from those in bulk water and in water in reverse micelles. This is indicated by the relatively long vibrational lifetime of the salt solution.

In addition to changes in the vibrational lifetime with reverse micelle size, the other significant difference observed in the population dynamics, compared to bulk water, is the long-lived component that exists following vibrational relaxation. In water (and in the 6 M NaCl solution, not shown), the signal decays to a constant nonzero value. However, in the reverse micelles, the long-lived signal decays. The pump−probe data for the 0−1 transition was fit with a biexponential functional form. One component was fixed at the lifetime obtained in fitting the 1−2 transition data. The second component was used to fit the residual pump−probe signal. The values obtained are also listed in Table 1. Figure 3 displays the pump−probe data along with the biexponential fits for the reverse micelle samples. As has been shown for bulk water[55] and methanol complexes in CCl_4,[78,79] the dynamics following vibrational relaxation can involve a complex kinetic scheme that includes the time for hydrogen bonds to break following vibrational relaxation. To fully detail the kinetics, a subsequent study will investigate the full wavelength dependence of the time-dependent spectrum, as has been done for bulk water.[55] Here, the results of the biexponential fits will be used to address the question of why the long-lived component decays in the reverse micelles but is constant in bulk water (see Figure 2). Because a full kinetic scheme was not used, there is some error in the fits at intermediate times. To obtain an accurate determination of the long-time components, fits were forced to reproduce the long-time portion of the data, even if that produced some error at shorter times.

In bulk water, thermal diffusion away from the local hot spots produced by vibrational relaxation cools the hot spots but heats the surrounding water. The shape of the temperature difference spectrum of bulk water (the spectrum obtained by subtracting the spectrum taken at a lower temperature from one taken at a higher temperature) is independent of the temperature difference for temperatures within tens of degrees around room temperature.[23] In bulk water, the cooling of the local hot spots, which reduces the amplitude of the photoproduct spectrum is offset by the increase in temperature of the surrounding water molecules, which then contribute to the photoproduct spectrum. The result is a constant long-lived signal for times greater than ~5 ps.

The reverse micelles are fundamentally different. The OD stretch is only contained in the water nanopools in the reverse micelles, and the reverse micelles are relatively far apart. On average, a given reverse micelle has, at most, one vibrational excitation per laser shot. Heat deposition in the reverse micelles, following vibrational relaxation, shifts the spectrum to that appropriate for the increase local temperature. The shift happens because of a reduction in the average number of hydrogen bonds.[23] However, thermal diffusion causes heat to flow out of the nanopool into the surfactant and the surrounding solvent. As heat flows out of the nanopools, reequilibration of the nanopool hydrogen-bond network reduces the amplitude of the long-lived signal. As the nanopool becomes smaller, the distance that must be traversed to move heat out of the water pool and into the surroundings decreases. It is proposed that the reduction in distance as the size decreases, and the concomitant decrease in the time required for heat to move out of the nanopools, is responsible for the decrease in the long decay time with reduced size. If the reequilibration is fast, compared to the temperature change, the decays shown in Figure 3 and the values listed Table 1 reflect the heat flow out of the nanopool. In bulk water, the hydrogen-bond equilibration time is fast (1.5 ps). However, as discussed below in connection with the analysis of the vibrational echo experiments, equilibration may slow substantially in the reverse micelles, in which case, the long time component of the decays in Figure 3 are a combination of heat flow and reequilibration. This picture of heat diffusion out of the reverse micelles, thereby causing the long-lived signal to decay, is consistent with observations of hydrogen-bond dissociation and reformation dynamics of methanol oligomers in CCl_4.[78]

It is interesting to contrast these results with those presented by Dlott and co-workers,[45] who examined the vibrational cascade of the excited OH stretch of H_2O in AOT reverse micelles. The experiments measure the vibrational relaxation of two different fundamental transitions: the OD stretch of HOD in the experiments described in this paper and the OH stretch of H_2O in the work presented by Dlott and co-workers.[45] Hence, direct comparisons cannot be made, because the vibrational relaxation process is dependent on the details of lower-frequency modes that are coupled to the initial vibrational excitation. The OH stretch of H_2O can have a fundamentally different relaxation pathway than the OD stretch of HOD. In addition, the excited OH stretch of H_2O in H_2O can undergo excitation transfer, whereas the excited OD stretch of HOD that is dilute in H_2O will not undergo excitation transfer. A qualitative comparison of the vibrational relaxation shows that similar trends are observed in the two experiments. Dlott and co-workers[45] reported a factor of 2.5 increase in the vibrational lifetime of the OH stretch when confined to a $w_0 = 2$ reverse micelle. We observe a factor of 4 difference when comparing the lifetime of HOD in bulk water versus HOD in the $w_0 = 2$ reverse micelle. The experiments presented here do not examine what fraction of the vibrational energy following relaxation goes into the water, relative to the headgroups/surfactants, and Dlott and co-workers[45] do not address the dynamics of the energy that

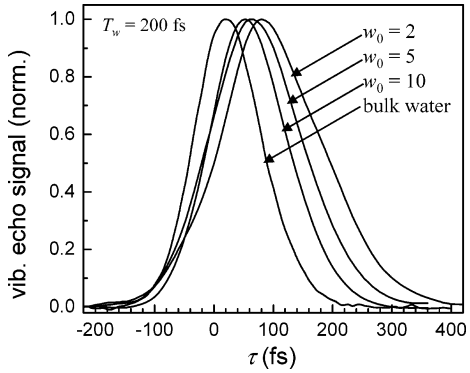

Figure 4. Normalized frequency resolved vibrational echo signals with $T_w = 200$ fs for bulk water and water in $w_0 = 10$, 5, and 2 AOT reverse micelles. For each sample, data were taken at the peak of the absorption spectrum.

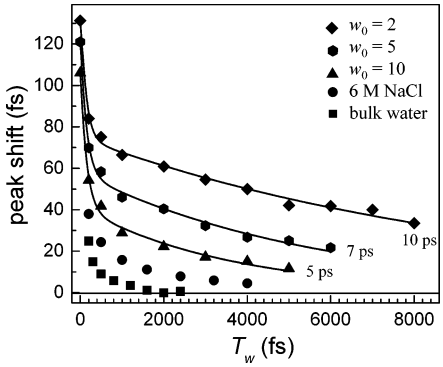

Figure 5. Vibrational echo peak shift data for all samples studied. The peak shift at $T_w = 0$ fs is reported for the three reverse micelle samples. Empirical biexponential curves (solid curves) are used to fit the reverse micelle data initially (see text).

does flow into the water. It is clear from the experiments presented here that a fraction of the energy goes into the water. Upon thermalization (tens of picoseconds), any residual pump−probe signal reflects heat in the water nanopools that slowly diffuses outward and that rate of return to the initial pre-excitation conditions is dependent on the size of the reverse micelle. It is possible that the partitioning of vibrational energy upon relaxation between the headgroups/surfactants and water is very different for the OH stretch of H_2O and the OD stretch of HOD.

In principle, vibrational relaxation contributes to the dynamics measured in vibrational echo experiments. However, the contribution to the dynamic line width (related to the Fourier transform of the vibrational echo decay) is not large on any time scale. The contribution from vibrational relaxation is given by $1/(2\pi T_1)$. Even for bulk water ($T_1 = 1.5$ ps), the lifetime contribution is only 3.5 cm^{-1} out of a total line width of ∼170 cm^{-1}. Therefore, any uncertainty in the lifetimes introduced by the generation of photoproducts, which necessitates measurement of the lifetime using the 0−1 transition, does not influence the analysis of the vibrational echo data.

B. Vibrational Echo Experiments. Figure 4 displays spectrally resolved stimulated vibrational echo decay curves for the OD stretch of HOD in bulk water and in the nanopools of the three reverse micelles $w_0 = 10$, 5, and 2 (left to right).[49] The data are scans of τ for a fixed value of $T_w = 200$ fs. The detection wavelength is located at the peak of the absorption spectrum (see Figure 1) for each sample. In going from bulk water to increasingly smaller nanopools, the decays become slower and the peaks of the decays move out to longer time. These data are an initial demonstration that the dynamics of water in reverse micelle nanopools are slower than those in bulk water and become progressively slower as the size of the reverse micelle is decreased.

The data reported here is spectrally resolved and taken at the peak of the absorption spectra for several reasons. Spectral resolution at the peak of the spectrum eliminates contributions from the 1−2 transition, because the anharmonicity is sufficiently large (162 cm^{-1} for bulk water[69]), compared to the absorption line width that there is little overlap at the peak of the ground-state absorption.[23,69,86] Inclusion of contributions to the signal from the 1−2 transition adds ambiguity to the data analysis. In addition, distinct subensembles of water molecules (that is, core versus waters associated with the headgroups) may have distinct dynamics that would be manifested in a study of the decays as a function of the detection wavelength. Preliminary evidence of such a wavelength dependence is presented below.

Data such as those displayed in Figure 4 were taken in all five samples over a range of T_w values. Each T_w value yields a distinct curve. The curves can be characterized by their shapes and their peak shifts. The peak shift is the displacement of the peak of the decay curve from the absolute position of $\tau = 0$, which is determined by a cross-correlation experiment on a nonresonant sample (no OD) with everything else being identical. As discussed in Section II, a procedure is used that ensures that the position of $\tau = 0$ is known accurately. First, the data on the five samples will be discussed qualitatively in terms of the peak shifts. As discussed further below, the peak shifts as well as the detailed shape of the decay curves can be calculated using a model FFCF within the Gaussian approximation. Therefore, the peak shifts are an observable related to the underlying dynamics of the system.

Figure 5 displays peak shift data (from bottom to top) for bulk water, 6 M NaCl solution, and water in nanopools for the $w_0 = 10$, 5, and 2 reverse micelles. The curves through the reverse micelle data are phenomenological biexponential fits and are not a diagrammatic perturbation theory[64] analysis of the data, which will be presented below. The vibrational echo peak shifts, as a function of T_w, are related to the decay of the FFCF.[87] The data in this form enable the qualitative trends to be observed prior to the detailed analysis. The peak shift results show that the bulk water dynamics are much faster than the water dynamics of the largest reverse micelle, $w_0 = 10$, for which the nanopool diameter is ∼4 nm and contains ∼1000 water molecules. When the peak shift decays to zero, spectral diffusion is complete, and the hydroxyl stretch oscillator has sampled the entire range of frequencies in the linear absorption line. Therefore, the full array of hydrogen-bond network configurations has been sampled. In contrast to bulk water, the peak shifts for the reverse micelles have not decayed to zero over the range of times investigated in the experiments. As the nanopool becomes smaller, the peak shift decay slows, demonstrating that the sampling of water structural configurations has slowed.

Experiments have shown that the presence of ions can affect some aspects of bulk water dynamics.[85] If the ionic headgroups and the Na^+ counterions were free ions in bulk water with the same number of ions per water molecule, the ionic strength for a $w_0 = 10$ reverse micelle would be equivalent to an ∼5.6 M NaCl solution. The vibrational lifetime in the NaCl solution is more than a factor of 2 longer than in bulk water (see Table 1). The vibrational echo peak shift data show that the high ionic strength of the 6 M NaCl solution does have an influence on the vibrational echo decay, slowing the decay compared to bulk water. However, the $w_0 = 10$ decay is even slower. The NaCl

solution data gives a long-time component of 2.1 ps, compared to 5 ps for $w_0 = 10$. Furthermore, simulations show that the Na ions are associated with the headgroups.[28] Consequently the ionic strength of the nanoscopic water is much lower than 5.6 M, and the influence of free ions in the water nanopools on the vibrational echo decay will be much less than that measured for the 6 M NaCl solution.

It is straightforward to understand why the ionic headgroups and the counterions are associated in a reverse micelle. For a $w_0 = 10$ micelle, the radius of the water pool is ~2 nm, and there is a spherical shell of ~100 surfactant headgroup negative ions surrounding the pool. If the 100 Na^+ counterions were randomly distributed in the water pool, then their average separation would be 0.8 nm. However, the Onsager length (r_c)[88] for water is 0.7 nm. The Onsager length reflects the separation necessary for the Coulomb interaction of a pair of charges to be screened by a dielectric solvent. The interaction of a pair of charges decreases exponentially with distance, and the Onsager length is the decay constant in the exponential. If ions are separated by 3 or 4, r and then the Coulomb interaction will be effectively screened out. Therefore, the 100 positive charges are not screened from each other or from the negative charges by the dielectric medium. The Na^+ ions will repel and be driven to the negative headgroup charges. This is in contrast to a bulk NaCl solution in which the positive and negative charges are intermixed, balancing the repulsive and attractive interactions.

In addition, IR pump−probe vibrational lifetime and orientation relaxation measurements made on the azide ion in reverse micelles with *uncharged headgroups* display a substantial slowing of both the lifetime and the orientational relaxation compared to bulk water.[42] When the nanopools in nonionic reverse micelles are decreased in size, the observed dynamics become increasingly slow. This is the same trend observed here on measurements made directly on the water molecules. The vibrational echo experiments on the 6 M NaCl solution, the simulations, and experiments on nonionic reverse micelles combine to demonstrate that the differences in the dynamics of nanoscopic water in AOT reverse micelles, compared to bulk water, are not significantly a result of ions dispersed in the aqueous phase disrupting the hydrogen bond network.

From Figure 4, it is clear that the dynamics of nanoscopic water in reverse micelles are very different from that of bulk water. The dynamics slow as the reverse micelle size is decreased. For example, at $T_w = 4$ ps, the peak shifts for $w_0 =$ 10, 5, and 2 are 20, 30, and 50 fs, respectively. The long components of the empirical fits to the decays in Figure 1 are 5, 7, and 10 ps for $w_0 = 10$, 5, and 2, respectively. Theory has shown that after the FFCF has decayed substantially, the peak-shift data decays in a manner that is equivalent to the FFCF.[87] Therefore, the long component of the empirical fits to the peak shift data should be similar to the FFCF determined by theoretical calculations if there has been sufficient decay. As shown below, the long time decay values given in Figure 5 are quite close to those obtained from detailed fits for $w_0 = 10$ and 5, but the value for $w_0 = 2$ is approximately a factor of 2 too fast. To obtain a more detailed understanding of the water dynamics in reverse micelles, the data were analyzed using time-dependent diagrammatic perturbation theory.[64]

Several types of data were calculated with diagrammatic perturbation theory.[64] To obtain the FFCF, the vibrational echo time-dependent decays over the range of T_w values and the linear absorption spectrum were fit simultaneously for each w_0 using an iterative algorithm that included the finite laser pulse duration. The resulting FFCF was then used to calculate the vibrational

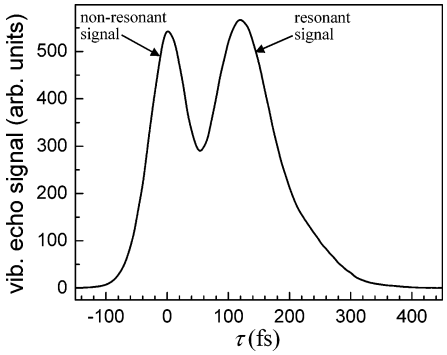

Figure 6. Vibrational echo decay curve for $w_0 = 5$ at $T_w = 0$ fs. The nonresonant signal at $\tau = 0$ fs influences the shape of the resonant vibrational echo decay curve although the vibrational echo peak shift is large enough to determine its value with reasonable accuracy.

echo peak shifts with no adjustable parameters. In accord with recent theoretical analysis and simulations of vibrational echo experiments of bulk water,[20] a triexponential form for the FFCF,

$$C(t) = \Delta_1^2 e_1^{-t/\tau} + \Delta_2^2 e_2^{-t/\tau} + \Delta_3^2 e_3^{-t/\tau} \quad (4)$$

was used. The Δ_i values are amplitude factors, given in units of frequency. The triexponential form comes from analysis of the FFCFs obtained from three distinct water simulations: TIP4P, SPC/E, and SPC-FQ.[20,69,71] In each case, the numerical FFCF obtained from the simulations could be fit very well with a triexponential of the form given by eq 4. We found that we could not fit all of the data nearly as well with a simpler form, using only two terms in the FFCF.

To fit the data, an initial guess of the FFCF was input into a fitting routine that calculates the vibrational echo decay curves over the range of T_w values measured and the linear absorption spectrum. The diagrammatic perturbation theory calculations used all eight relevant diagrams and the measured pulse duration. The resulting calculated curves and the data were used to determine the sum of the square of the residuals (χ^2) and the FFCF was then iterated to minimize χ^2. For each nanopool size, the data were fit out to as long a T_w as could be measured. However, data at $T_w = 0$ were not used in any of the fits, because of the large nonresonant contribution at $\tau = 0$. Figure 6 shows data for $w_0 = 5$ at $T_w = 0$. The nonresonant peak centered at $\tau = 0$ results mainly from the CCl_4 solvent. CCl_4 is very polarizable and, therefore, results in a large nonresonant signal. Although the nonresonant signal is well-separated from the resonant signal, clearly the shape cannot be fit. Furthermore, there is some ambiguity in the peak shift. The value of the peak shift at $T_w = 0$ is still useful, even if it contains some uncertainty, because it permits the extent of the decay at early times to be known. For example, in Figure 3, the $w_0 = 10$ data have decayed from ~106 fs at $T_w = 0$ to ~10 fs at $T_w = 5$ ps. Figure 7 displays the data and fit for $w_0 = 5$ and $T_w = 200$ fs. The fit is slightly too slow on the rising edge and slightly too fast on the falling edge; however, overall, the fits are very good, except for $w_0 =$ 2, as discussed below.

Figure 8 shows the vibrational echo peak shift data and the calculated peak shifts obtained using the FFCF determined from the global fits to the decay curves over the range of T_w values and the linear line shape. There are no adjustable parameters in the peak shift calculations. The determination of the FFCF did not include the $T_w = 0$ fs data for the reasons discussed previously. The FFCFs that result in the solid lines are given in Table 2. Table 2 also contains the parameters for bulk water and the 6 M NaCl solution.

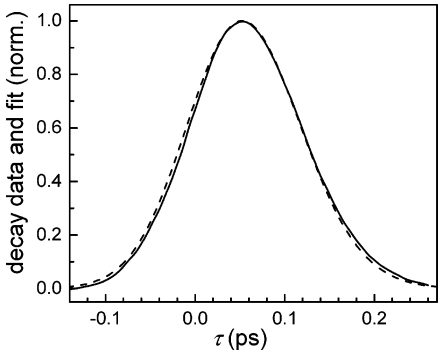

Figure 7. $T_w = 200$ fs, $w_0 = 5$ vibrational echo data (solid curve) and the calculated curve (dashed curve) obtained from the frequency−frequency correlation functions (FFCF) (Table 2) determined by the fit to data for multiple T_w values and the linear line shape.

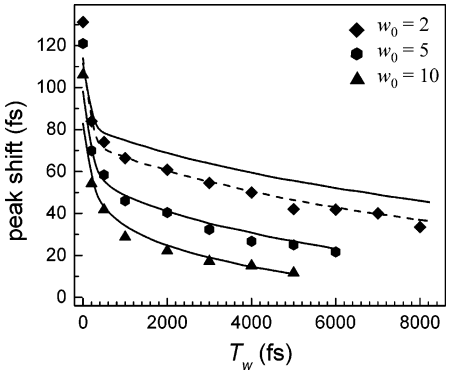

Figure 8. Vibrational echo peak shift data for all reverse micelle samples with calculated curves (solid curves) obtained with no adjustable parameters from the using the FFCFs determined from fits to the decay curves shapes and linear absorption spectrum. For $w_0 = 10$ and 5, the agreement is good. For $w_0 = 2$, the shape of the decay is good, but the amplitude misses by ∼10 fs at longer times. The dashed curve is a fit to the peak shift data for $w_0 = 2$. The FFCF parameters used to calculate the curves are given in Table 2.

TABLE 2: Frequency−Frequency Correlation Function (FFCF) Parameters Used in eq 5

sample	Δ_1 (cm^{-1})	τ_1 (ps)	$1/(\pi T_2^*)^a$ (cm^{-1})	Δ_2 (cm^{-1})	τ_2 (ps)	Δ_3 (cm^{-1})	τ_3 (ps)
bulk water[a]	60	0.045	61	20	0.41	55	1.5
6 M NaCl	74	0.027	56	22	0.32	50	2.1
$w_0 = 10$	59	0.033	42	35	0.46	61	5[b]
$w_0 = 5$	38	0.054	30	28	0.27	47	8[b]
$w_0 = 2$	35	0.065	30	15	0.16	51	22[b]
$w_0 = 2$ (peak shift)	28	0.11	32	22	0.15	44	16[b]

[a] Obtained from other experiments (see refs 20 and 69). [b] Error bars represent the random error (±1 ps). For $w_0 = 2$, two values are obtained, depending on which experimental observable is fit (see text). The difference is not a random error.

First consider the $w_0 = 10$ and 5 reverse micelles. The calculations based on the experimentally determined FFCFs for these two reverse micelles do a very good job of reproducing the peak shift data. The longest component is the same or similar to that determined by the empirical fits shown in Figure 5. The slowest component for the $w_0 = 10$ and 5 reverse micelles are 5 and 8 ps, respectively. Both are much slower than the slowest component for bulk water (1.5 ps) (see Table 2). The calculated curves miss the $T_w = 0$ fs points by ∼20 fs; however, these points were not in the fits, and their experimental values are uncertain, to some extent. The results demonstrate that the calculations are able to reproduce the shapes of the decay curves at all T_w values quite accurately, and thereby obtain an FFCF that reproduces the peak shifts. It is unlikely that there is a slower component of any substantial size that was missed. The $w_0 = 10$ peak shift begins at ∼106 fs and by the last data point, it is down to ∼10 fs. The data and the calculated curve both have a downward slope. Therefore, if there is a longer time scale component not contained in the three terms of eq 4, its amplitude is very small. The same argument holds true for $w_0 = 5$, where the initial peak shift is ∼120 fs and the last data point is ∼20 fs, with the data and the calculated curve having a downward slope.

The solid line for $w_0 = 2$, calculated by fitting the shapes of the decay curves and the linear absorption spectrum, reproduces the form of the time dependence of the peak shift data but misses the values by ∼10 fs at the longer times. This is because the FFCF form given in eq 4 does not reproduce the shape of the decay as well as the results shown in Figure 7 for $w_0 = 5$. The fit compromises the shape and misses the peak shifts somewhat. The dashed line is a fit to only the peak shifts. The FFCF parameters for both fits to the $w_0 = 2$ data are given in Table 2. The values obtained from the two fits are very similar, except for the longest component. For all of the samples, the first component of the FFCF is motionally narrowed. Therefore, the contribution to the vibrational echo decay from the first component is

$$T_2^* = \frac{1}{\Delta_1^2 \tau_1} \tag{5}$$

Δ_1 and τ_1 cannot be determined independently. The contribution to the dynamic line width for a motionally narrowed component is $1/(\pi T_2^*)$. For $w_0 = 2$, both sets of Δ_1 and τ_1 give almost the same motionally narrowed line width (∼30 cm^{-1}). Some amplitude is shifted from the slowest component, and τ_3 is reduced from 22 ps for the fit to the shapes to 16 ps for the fit to the peak shifts.

Table 2 gives the FFCFs obtained for all five samples. The expression $1/(\pi T_2^*)$ represents the width of the Lorentzian corresponding to the Fourier transform of the motionally narrowed decay. Bulk water and the NaCl solution have almost the same motionally narrowed component. The contribution to the dynamic line width from this component is smaller for the nanopools, but, at most, by a factor of 2, compared to bulk water. Within experimental error, the fast components of the $w_0 = 5$ and 2 reverse micelles are the same.

The triexponential form of the FFCF (eq 4) is obtained from fits to the numerical simulations of the bulk water FFCF. The simulations of bulk water reveal that there are two fundamentally distinct types of motions that contribute to the dynamics.[20,21,69] The very short time contributions result from very local motions associated with fluctuations in hydrogen-bond lengths and some changes in angles. The long time-scale motions are more global. They are hydrogen-bond equilibration, i.e., the making and breaking of hydrogen bonds. In the decomposition of the numerical FFCFs into triexponentials, the intermediate component should be considered to be a crossover between the two classes of dynamics. Vibrational echo correlation spectroscopy measurements on bulk water suggest that the time scale for the boundary between the two types of motions is ∼400 fs.[55] The values of the intermediate component of the FFCFs do not vary by a great amount, although τ_2 is faster for the smaller nanopools.

The most dramatic changes are in the long-time components of the FFCFs. Although the amplitudes of the long-time components of the FFCFs (Δ_3) for the five samples vary somewhat, the decay constant varies substantially. Going from

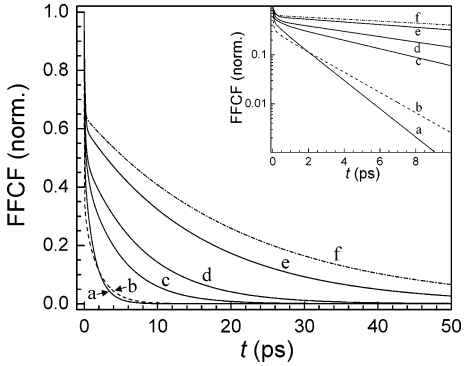

Figure 9. Normalized FFCFs for (a) bulk water, (b) 6 M NaCl solution, (c) the $w_0 = 10$ reverse micelle, (d) the $w_0 = 5$ reverse micelle, and (e, f) the $w_0 = 2$ reverse micelle. The two FFCFs for $w_0 = 2$ are from fits to the vibrational echo peak shifts (panel e) and the vibrational echo decay curve and linear absorption spectrum (panel f) (see Figure 6 and text). Inset: semilogarithmic plots of the same FFCFs.

bulk water to the $w_0 = 2$ reverse micelles, the long-time component slows by more than a factor of 10. Even the slowest component of the $w_0 = 10$ reverse micelle is more than a factor of 3 slower than that of bulk water. The slowest component of the NaCl solution is ~50% slower than that of bulk water. As discussed previously, the reverse micelle nanopools have the counterions associated with the headgroups; thus, the ionic strength is much less than that of the 6 M NaCl solution. In the reverse micelles, the consequence of confinement has a pronounced effect on τ_3. In this environment, water molecules are interacting with the headgroups and their associated counterions at the surfactant interface, and the water molecules are confined to a nanoscopic pool that has the effect of restricting their global motions.

Figure 9 displays the FFCFs given in Table 1 normalized to unity. The inset is a semilogarithmic plot of the same curves. The uppermost curves in both plots are the FFCFs for $w_0 = 2$, obtained by fitting the data using the two methods discussed previously, i.e., fitting the decay curve shapes (the uppermost curve, the dashed−dotted line) or fitting the peak shifts (second curve from top, solid line). The third and forth curves from the top are for the $w_0 = 5$ and 10 reverse micelles, respectively. The FFCFs for the water nanopools are very different from the bulk water and the NaCl solution FFCFs. The bulk water FFCF (fastest solid curve) is below the NaCl solution curve (dashed) at long time, but the reverse is true at short time. However, because the fastest components of all of the FFCFs reflect motionally narrowed dynamics, only $\Delta_1^2\tau_1$ can be determined from the data. Therefore, the very short time differences between bulk water and the NaCl solution are not significant. Only the $\Delta_1^2\tau_1$ values should be compared. These are given in Table 2, where it can be seen that the fast component of the decay for bulk water and the NaCl solution are very similar, with $1/(\pi T_2^*) = 61$ and 56 cm^{-1}, respectively. The important point is that, on all time scales, the FFCFs for bulk water and the NaCl solution decay substantially faster than those for the water nanopools. If, in analogy to bulk water, we identify the slowest component as resulting from hydrogen-bond equilibration, then confining water in nanoscopic pools has the effect of substantially slowing the rate of hydrogen-bond equilibration.

All of the values reported in Table 2 are from data taken at the peak of the absorption spectrum for each sample. Vibrational echo data taken at multiple frequencies have the potential of dynamically resolving the presence of multiple species that may not be resolvable using linear FTIR spectroscopy. From the FTIR spectra presented in Figure 1, it is not evident that multiple

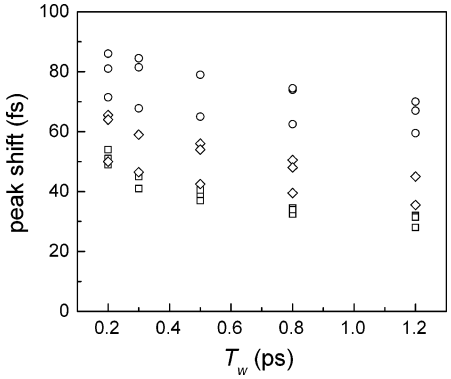

Figure 10. Peak shift vs T_w data for the three reverse micelles at three wavelengths: the center wavelength and wavelengths ~40 cm^{-1} to the red and blue of the absorption maximum. The square symbols are for $w_0 = 10$ (2495 cm^{-1}, 2535 cm^{-1}, 2575 cm^{-1}); the diamond symbols are for $w_0 = 5$ (2525 cm^{-1}, 2560 cm^{-1}, 2600 cm^{-1}); and the circle symbols are for $w_0 = 2$ (2535 cm^{-1}, 2575 cm^{-1}, 2615 cm^{-1}). Some of the data points are identical and do not appear as separate points. The smaller reverse micelles display a wavelength dependence (see text).

species of water exist within a reverse micelle. As mentioned previously, water in reverse micelles is frequently separated into water molecules in the core of the reverse micelle (which are described as "free" water) and water molecules that are associated with the headgroups. This separation into two classes of water molecules has been used by many experimentalists and theoreticians to aid in explaining data and simulations of water in reverse micelles.[27,28,31,38,89] Simulations indicate that the different classes of water have distinct dynamics. To address the possibility that the different classes of water molecules have distinct dynamics, we performed an initial study of the wavelength dependence of the vibrational echo decays.

Figure 10 displays peak shift data for a series of decay curves taken at relatively short T_w values for the three reverse micelles at three wavelengths: the center wavelength and wavelengths ~40 cm^{-1} to the red and blue of the absorption maximum. The square symbols represent the $w_0 = 10$ (2495 cm^{-1}, 2535 cm^{-1}, 2575 cm^{-1}) data, the diamond symbols represent $w_0 = 5$ (2525 cm^{-1}, 2560 cm^{-1}, 2600 cm^{-1}); and the circle symbols represent $w_0 = 2$ (2535 cm^{-1}, 2575 cm^{-1}, 2615 cm^{-1}). At each time point, there are three data points for each sample. Some of the data points are identical and do not appear as separate points. The data for $w_0 = 10$ (squares) are identical, within experimental error. However, for $w_0 = 5$ and $w_0 = 2$, there is a clear wavelength dependence. For each of the smaller reverse micelles, the center wavelength data and the red wavelength data are the same within experimental error. However, the blue wavelength data have a smaller associated peak shift and are distinct with the differences well outside of experimental error.

The wavelength dependence of the vibrational echo data for the two smaller reverse micelles suggests that there are different subensembles of water that are dynamically distinct. For the $w_0 = 10$ reverse micelle, approximately half of the water molecules reside in the first solvation shell of the surfactant headgroups. If the classification of associated versus core water molecules is meaningful, then 50% of the water molecules in the $w_0 = 10$ reverse micelle are associated and 50% are core. In this reverse micelle, wavelengths near the center of the spectrum may not contain sufficient contribution from associated waters for a difference to be observed if the associated waters are blue-shifted from the core waters. In the two smaller reverse micelles, the dynamics differ when the wavelength is shifted to the blue. If the associated waters have fewer and/or weaker hydrogen bonds, their absorption would be expected to be blue-

shifted. In the smaller reverse micelles, the relative portion of associated water, compared to that of core waters, is larger. Recently, it has been suggested that water can be classified into three populations: associated, core, and "trapped".[28] The trapped water refers to molecules that reside within the headgroup region and may not interact with other water molecules. It is possible that the hydrogen-bond dynamics of associated and core waters are indistinguishable, whereas it is the dynamics of the trapped water molecules that are distinct and observed at the shorter wavelengths. Because the number of trapped water molecules, relative to the associated and core water population is small, the wavelength dependence might only be observed for the smallest reverse micelles.

We are currently preparing to do fully frequency-dependent studies. Because each frequency is an entire experiment, currently the time involved is prohibitive. Relatively soon, we will have a 32-element array detector available to using in making the wavelength-dependent measurements. This will enable us to measure 32 wavelengths at once, making a detailed wavelength-dependent study feasible.

IV. Concluding Remarks

Ultrafast infrared (IR) spectrally resolved pump−probe and stimulated vibrational echo experiments were performed on the OD stretch of HOD in water of nanoscopic dimensions in reverse micelles. The experiments probe the dynamics of water molecules in a confined environment.

The pump−probe spectroscopy of water, as well as that of water in reverse micelles, is complicated by hydrogen-bond equilibration dynamics following vibrational relaxation. The biexponential pump−probe decays have a short-time component that is caused by vibrational relaxation and a long-time component that is caused by a thermally induced shift in the hydrogen-bond distribution that recovers as a result of the energy diffusing out of the reverse micelle. As the water nanopool becomes smaller, the vibrational lifetime becomes long, but the long component becomes shorter. The decay of the long-lived component is distinct from the pump−probe signal for bulk water, which does not decay until heat has diffused out of the excited laser volume.

The vibrational echo experiments examine the dynamics of the hydrogen-bond network evolution through the influence of structural changes on the hydroxyl stretch vibrational frequency. The results show that the fastest dynamics are only mildly different from bulk water; however, the longer-time-scale dynamics are more than an order of magnitude slower than those observed for bulk water. The results of this work, simulations,[28] and the work on nonionic reverse micelles[41,42] demonstrate that the differences between nanoscopic water and bulk water measured here are not caused by ionic strength effects.

Drawing upon water simulations provides insights into the changes in dynamics observed in reverse micelle nanopools. The parameters for the triexponential form of the water FFCF are given in Table 2.[20,69] In the simulations of water, this fastest component is identified as the very local fluctuations of the lengths of the hydrogen bonds.[18,20−22] The slowest component has been associated with more global structural evolution of the hydrogen-bonding network, i.e., the making and breaking of hydrogen bonds (hydrogen-bond equilibration).[18,20−22] Simulations of the FFCF of nanoscopic water in reverse micelles have not yet been performed. At this time, we can only compare to simulations of bulk water by assuming that the nature of the dynamics are the same. The slowest component of the water nanopool FFCF has the largest difference, when compared to bulk water. Although the amplitudes of the slowest component (Δ_3) are similar, the decay time (τ_3) is much longer in the nanopools than in bulk water. The increasing τ_3 value with decreasing w_0 value, and, hence, a lengthening of the time for hydrogen-bond equilibration, may be associated with the inability of water molecules to move, relative to each other. This is consistent with a reduction in translational and rotational mobility,[47] both from confinement as well as the increasing presence of water molecules interacting with the reverse micelle interface.[28,31,42]

The direct measurements of the nanoscopic water dynamics presented here are in accord with the general trends observed in previous time-resolved experiments on probe molecules in reverse micelles.[31,42] Wavelength-dependent studies of the vibrational echo signal indicate a frequency dependence for the smaller $w_0 = 5$ and $w_0 = 2$ reverse micelles. The peak shifts of the vibrational echo decays for the bluest frequencies occur more rapidly at short times. The unusual frequency dependence of the vibrational echo data may be a result of the observation of more than one ensemble of water molecules, that is, associated and core waters. A fully wavelength-dependent study may be able to determine the spectra of the subensembles, using dephasing selectivity to separate the spectral features.

Nanoscopic water occurs in many physical systems. The AOT reverse micelles have ionic headgroups. Experiments on larger AOT reverse micelles are in progress to investigate the approach to bulklike behavior. In addition, experiments have begun to study nanoscopic water in reverse micelles with nonionic headgroups, in sol−gel glasses, and in Nafion ion-exchange membranes. By contrasting the results from different types of systems, a deeper understanding of the nanoscopic water will be obtained. To compliment the experimental studies, simulations of the experimental observables will be pursued to provide a microscopic understanding of the dynamics in water nanopools.

Acknowledgment. This work was supported by the Department of Energy (under Contract No. DE-FG03-84ER13251), the National Institutes of Health (under Grant No. 2R01GM-061137-05), and the National Science Foundation (under Grant No. DMR-0332692).

References and Notes

(1) Habuchi, S.; Kim, H. B.; Kitamura, N. *Anal. Chem.* **2001**, *73*, 366.
(2) Pal, S. K.; Zewail, A. H. *Chem. Rev.* **2004**, *104*, 2099.
(3) Sutton, R.; Sposito, G. *J. Colloid Interface Sci.* **2001**, *237*, 174.
(4) Nandi, N.; Bagchi, B. *J. Phys. Chem. B* **1997**, *101*, 10954.
(5) Pillai, V.; Kumar, P.; Hou, M. J.; Ayyub, P.; Shah, D. O. *Adv. Colloid Interface Sci.* **1995**, *55*, 241.
(6) Biswas, R.; Pal, S. K. *Chem. Phys. Lett.* **2004**, *387*, 221.
(7) Beta, I. A.; Bohlig, H.; Hunger, B. *Phys. Chem. Chem. Phys.* **2004**, *6*, 1975.
(8) Cameron, I. L.; Kanal, K. M.; Keener, C. R.; Fullerton, G. D. *Cell Biol. Int.* **1997**, *21*, 99.
(9) Nandi, N.; Bhattacharyya, K.; Bagchi, B. *Chem. Rev.* **2000**, *100*, 2013.
(10) Levinger, N. E. *Science* **2002**, *298*, 1722.
(11) Loughnane, B. J.; Farrer, R. A.; Scodinu, A.; Reilly, T.; Fourkas, J. T. *J. Phys. Chem. B* **2000**, *104*, 5421.
(12) Bhattacharyya, K. *Acc. Chem. Res.* **2003**, *36*, 95.
(13) Vajda, S.; Jimenez, R.; Rosenthal, S. J.; Fidler, V.; Fleming, G. R.; Castner, E. W. *J. Chem. Soc. Faraday Trans.* **1995**, *91*, 867.
(14) Schuster, P.; Zundel, G.; Sandorfy, C. *The Hydrogen Bond. Recent Developments in Theory and Experiments*; North−Holland: Amsterdam, 1976.
(15) Bakker, H. J.; Neinhuys, H. K.; Gallot, G.; Lascoux, N.; Gale, G. M.; Leicknam, J. C.; Bratos, S. *J. Chem. Phys.* **2002**, *116*, 2592.
(16) Stenger, J.; Madsen, D.; Hamm, P.; Nibbering, E. T. J.; Elsaesser, T. *J. Phys. Chem. A* **2002**, *106*, 2341.

(17) Yeremenko, S.; Pshenichnikov, M. S.; Wiersma, D. A. *Chem. Phys. Lett.* **2003**, *369*, 107.
(18) Fecko, C. J.; Eaves, J. D.; Loparo, J. J.; Tokmakoff, A.; Geissler, P. L. *Science* **2003**, *301*, 1698.
(19) Nibbering, E. T. J.; Elsaesser, T. *Chem. Rev.* **2004**, *104*, 1887.
(20) Asbury, J. B.; Steinel, T.; Stromberg, C.; Corcelli, S. A.; Lawrence, C. P.; Skinner, J. L.; Fayer, M. D. *J. Phys. Chem. A* **2004**, *108*, 1107.
(21) Lawrence, C. P.; Skinner, J. L. *J. Chem. Phys.* **2003**, *118*, 264.
(22) Møller, K. B.; Rey, R.; Hynes, J. T. *J. Phys. Chem. A* **2004**, *108*, 1275.
(23) Steinel, T.; Asbury, J. B.; Fayer, M. D. *J. Phys. Chem. A* **2004**, *108*, 10957.
(24) Woutersen, S.; Bakker, H. J. *Nature (London)* **1999**, *402*, 507.
(25) Woutersen, S.; Emmerichs, U.; Nienhuys, H.-K.; Bakker, H. J. *Phys. Rev. Lett.* **1998**, *81*, 1106.
(26) Maitra, A. *J. Phys. Chem.* **1984**, *88*, 5122.
(27) Onori, G.; Santucci, A. *J. Phys. Chem.* **1993**, *97*, 5430.
(28) Faeder, J.; Ladanyi, B. M. *J. Phys. Chem. B* **2000**, *104*, 1033.
(29) Senapati, S.; Berkowitz, M. L. *J. Phys. Chem. A* **2004**, *108*, 9768.
(30) Das, K.; Sarkar, N.; Das, S.; Datta, A.; Bhattacharyya, K. *Chem. Phys. Lett.* **1996**, *249*, 323.
(31) Riter, R. E.; Willard, D. M.; Levinger, N. E. *J. Phys. Chem. B* **1998**, *102*, 2705.
(32) Kotlarchyk, M.; Huang, J. S.; Chen, S.-H. *J. Phys. Chem.* **1985**, *89*, 4382.
(33) Bohidar, H. B.; Behboudnia, M. *Colloids Surf., A* **2001**, *178*, 313.
(34) D'Angelo, M.; Fioretto, D.; Onori, G.; Palmieri, L.; Santucci, A. *Phys. Rev. E* **1996**, *54*, 993.
(35) Boyd, J. E.; Briskman, A.; Colvin, V. L.; Mittleman, D. M. *Phys. Rev. Lett.* **2001**, *87*, 147401.
(36) Novaki, L. P.; El Seoud, O. A. *J. Colloid Interface Sci.* **1998**, *202*, 391.
(37) Christopher, D. J.; Yarwood, J.; Belton, P. S.; Hills, B. P. *J. Colloid Interface Sci.* **1992**, *152*, 465.
(38) Venables, D. S.; Huang, K.; Schmuttenmaer, C. A. *J. Phys. Chem. B* **2001**, *105*, 9132.
(39) Willard, D. M.; Riter, R. E.; Levinger, N. E. *J. Am. Chem. Soc.* **1998**, *120*, 4151.
(40) Sarkar, N.; Das, K.; Datta, A.; Das, S.; Bhattacharyya, K. *J. Phys. Chem.* **1996**, *100*, 10523.
(41) Zhong, Q.; Baronavski, A. P.; Owrutsky, J. C. *J. Chem. Phys.* **2003**, *118*, 7074.
(42) Zhong, Q.; Baronavski, A. P.; Owrutsky, J. C. *J. Chem. Phys.* **2003**, *119*, 9171.
(43) Maekawa, H.; Ohta, K.; Tominaga, K. *Phys. Chem. Chem. Phys.* **2004**, *6*, 4074.
(44) Maekawa, H.; Ohta, K.; Tominaga, K. Vibrational Dynamics of the OH Stretching Mode of Water in Reverse Micelles Studied by Infrared Nonlinear Spectroscopy. *Mater. Res. Soc. Symp. Proc.* **2003**, *790*.
(45) Deak, J. C.; Pang, Y.; Sechler, T. D.; Wang, Z.; Dlott, D. D. *Science* **2004**, *306*, 473.
(46) Harpham, M. R.; Ladanyi, B. M.; Levinger, N. E.; Herwig, K. W. *J. Chem. Phys.* **2004**, *121*, 7855.
(47) Tan, H.-S.; Piletic, I. R.; Fayer, M. D. *J. Chem. Phys.* **2005**, *122*, 174501(9).
(48) Ladanyi, B. M.; Skaf, M. S. *Ann. Rev. Phys. Chem.* **1993**, *44*, 335.
(49) Tan, H.-S.; Piletic, I. R.; Riter, R. E.; Levinger, N. E.; Fayer, M. D. *Phys. Rev. Lett.* **2004**, *94*, 057405(4).
(50) Zimdars, D.; Tokmakoff, A.; Chen, S.; Greenfield, S. R.; Fayer, M. D.; Smith, T. I.; Schwettman, H. A. *Phys. Rev. Lett.* **1993**, *70*, 2718.
(51) Tokmakoff, A.; Fayer, M. D. *J. Chem. Phys.* **1995**, *103*, 2810.
(52) Rector, K. D.; Fayer, M. D. *Laser Chem.* **1999**, *19*, 19.
(53) Hamm, P.; Lim, M.; Hochstrasser, R. M. *Phys. Rev. Lett.* **1998**, *81*, 5326.
(54) Asbury, J. B.; Steinel, T.; Fayer, M. D. *J. Lumin.* **2004**, *107*, 271.
(55) Steinel, T.; Asbury, J. B.; Corcelli, S. A.; Lawrence, C. P.; Skinner, J. L.; Fayer, M. D. *Chem. Phys. Lett.* **2004**, *386*, 295.
(56) Stenger, J.; Madsen, D.; Hamm, P.; Nibbering, E. T. J.; Elsaesser, T. *Phys. Rev. Lett.* **2001**, *87*, 027401.
(57) Lawrence, C. P.; Skinner, J. L. *J. Chem. Phys.* **2002**, *117*, 8847.
(58) Asbury, J. B.; Steinel, T.; Stromberg, C.; Gaffney, K. J.; Piletic, I. R.; Goun, A.; Fayer, M. D. *Chem. Phys. Lett.* **2003**, *374*, 362.
(59) Asbury, J. B.; Steinel, T.; Stromberg, C.; Gaffney, K. J.; Piletic, I. R.; Fayer, M. D. *J. Chem. Phys.* **2003**, *119*, 12981.
(60) Piletic, I. R.; Gaffney, K. J.; Fayer, M. D. *J. Chem. Phys.* **2003**, *119*, 423.
(61) Gale, G. M.; Gallot, G.; Hache, F.; Lascoux, N.; Bratos, S.; Leicknam, J. C. *Phys. Rev. Lett.* **1999**, *82*, 1068.
(62) Woutersen, S.; Bakker, H. J. *Phys. Rev. Lett.* **1999**, *83*, 2077.
(63) Tokmakoff, A.; Fayer, M. D. *Acc. Chem. Res.* **1995**, *28*, 437.
(64) Mukamel, S. *Principles of Nonlinear Optical Spectroscopy*; Oxford University Press: New York, 1995.
(65) Pimentel, G. C.; McClellan, A. L. *The Hydrogen Bond*; W. H. Freeman and Co.: San Francisco, 1960.
(66) Liddel, U.; Becker, E. D. *Spectrochim. Acta* **1957**, *10*, 70.
(67) Mikenda, W. *J. Mol. Struct.* **1986**, *147*, 1.
(68) Novak, A. Hydrogen bonding in solids. In *Structure and Bonding*; Dunitz, J. D., Ed.; Springer−Verlag: Berlin, 1974; Vol. 18, p 177.
(69) Asbury, J. B.; Steinel, T.; Kwak, K.; Corcelli, S.; Lawrence, C. P.; Skinner, J. L.; Fayer, M. D. *J. Chem. Phys.* **2004**, *121*, 12431.
(70) Corcelli, S.; Lawrence, C. P.; Skinner, J. L. *J. Chem. Phys.* **2004**, *120*, 8107.
(71) Corcelli, S.; Lawrence, C. P.; Asbury, J. B.; Steinel, T.; Fayer, M. D.; Skinner, J. L. *J. Chem. Phys.* **2004**, *121*, 8897.
(72) Zulauf, M.; Eicke, H.-F. *J. Phys. Chem.* **1979**, *83*, 480.
(73) Kinugasa, T.; Kondo, A.; Nishimura, S.; Miyauchi, Y.; Nishii, Y.; Watanabe, K.; Takeuchi, H. *Colloid Surf. A* **2002**, *204*, 193.
(74) Izquierdo, C.; Moya, M. L.; Usero, J. L.; Casado, J. *Monatsh. Chem.* **1992**, *123*, 383.
(75) Tan, H.-S.; Piletic, I. R.; Fayer, M. D. *J. Opt. Soc. Am. B* **2005**, accepted.
(76) Merchant, K. A.; Thompson, D. E.; Fayer, M. D. *Phys. Rev. A* **2002**, *65*, 023817(16).
(77) Corcelli, S.; Skinner, J. L. *J. Chem. Phys.* **2005**, submitted.
(78) Gaffney, K. J.; Davis, P. H.; Piletic, I. R.; Levinger, N. E.; Fayer, M. D. *J. Phys. Chem. A* **2002**, *106*, 12012.
(79) Gaffney, K.; Piletic, I.; Fayer, M. D. *J. Phys. Chem. A* **2002**, *106*, 9428.
(80) Deak, J. C.; Rhea, S. T.; Iwaki, L. K.; Dlott, D. D. *J. Phys. Chem. A* **2000**, *104*, 4866.
(81) Oxtoby, D. W. *Annu. Rev. Phys. Chem.* **1981**, *32*, 77.
(82) Kenkre, V. M.; Tokmakoff, A.; Fayer, M. D. *J. Chem. Phys.* **1994**, *101*, 10618.
(83) Hadzi, D.; Thompson, H. W. *Hydrogen Bonding*; Pergamon Press, Ltd.: London, 1959.
(84) Mittleman, D. M.; Nuss, M. C.; Colvin, V. L. *Chem. Phys. Lett.* **1997**, *275*, 332.
(85) Kropman, M. F.; Bakker, H. J. *Science* **2001**, *291*, 2118.
(86) Xu, Q.-H.; Thompson, D. E.; Merchant, K. A.; Fayer, M. D. *Chem. Phys. Lett.* **2002**, *355*, 139.
(87) Cho, M. H.; Yu, J. Y.; Joo, T. H.; Nagasawa, Y.; Passino, S. A.; Fleming, G. R. *J. Chem. Phys.* **1996**, *100*, 11944.
(88) Onsager, L. *Phys. Rev.* **1938**, *54*, 554.
(89) Bhattacharyya, K.; Bagchi, B. *J. Phys. Chem. A* **2000**, *104*, 10603.